Purdue University
Purdue e-Pubs

Birck and NCN Publications | Birck Nanotechnology Center

8-1-2008

Titanium-based dielectrophoresis devices for microfluidic applications

Y T. Zhang
Univ Calif Santa Barbara

F Bottausci
Univ Calif Santa Barbara

Masaru P. Rao
Birck Nanotechnology Center, Purdue University, mprao@purdue.edu

E R. Parker
Univ Calif Santa Barbara

N C. MacDonald
Univ Calif Santa Barbara

Follow this and additional works at: http://docs.lib.purdue.edu/nanopub

Zhang, Y T.; Bottausci, F; Rao, Masaru P.; Parker, E R.; and MacDonald, N C., "Titanium-based dielectrophoresis devices for microfluidic applications" (2008). *Birck and NCN Publications.* Paper 150.
http://docs.lib.purdue.edu/nanopub/150

This document has been made available through Purdue e-Pubs, a service of the Purdue University Libraries. Please contact epubs@purdue.edu for additional information.

Biomed Microdevices (2008) 10:509–517
DOI 10.1007/s10544-007-9159-y

Titanium-based dielectrophoresis devices for microfluidic applications

Y. T. Zhang · F. Bottausci · M. P. Rao · E. R. Parker · I. Mezic · N. C. MacDonald

Published online: 23 January 2008
© Springer Science + Business Media, LLC 2008

Abstract To date, materials selection in microfluidics has been restricted to conventional micromechanical materials systems such as silicon, glass, and various polymers. Metallic materials offer a number of potential advantages for microfluidic applications, including high fracture toughness, thermal stability, and solvent resistance. However, their exploitation in such applications has been limited. In this work, we present the application of recently developed titanium micromachining and multilayer lamination techniques for the fabrication of dielectrophoresis devices for microfluidic particle manipulation. Two device designs are presented, one with interdigitated planar electrodes defined on the floor of the flow channel, and the other with electrodes embedded within the channel wall. Using these devices, two-frequency particle separation and Z-dimensional flow visualization of the dielectrophoresis phenomena are demonstrated.

Y. T. Zhang (✉) · F. Bottausci · E. R. Parker · I. Mezic · N. C. MacDonald
Mechanical and Environmental Engineering Department,
University of California, Santa Barbara (UCSB),
Santa Barbara, CA 93106, USA
e-mail: zhyt@engr.ucsb.edu

M. P. Rao
School of Mechanical Engineering,
School of Materials Engineering, Birck Nanotechnology Center,
Center for Advanced Manufacturing, Purdue University,
585 Purdue Mall,
West Lafayette, IN 47907-2088, USA
e-mail: mprao@purdue.edu

N. C. MacDonald
Materials Department, University of California,
Santa Barbara (UCSB),
Santa Barbara, CA 93106, USA

Keywords Bulk titanium · Microfabrication · Dielectrophoresis · Sidewall electrodes · μPIV · Microfluidics

1 Introduction

Microfluidics has shown significant promise as a technological platform for reducing cost and enhancing speed, sensitivity, and efficiency of a wide range of chemical, biological, and biomedical analyses (Ho and Tai 1998; Figeys and Pinto 2000; Stone et al. 2004). This diversity of applications has motivated the concomitant development of a variety of micromechanical materials systems, including silicon, glass, and various polymers. Silicon and glass-based devices were predominant early in the history of microfluidics, due to the reliance upon fabrication techniques derived from the microelectronics manufacturing area. However, polymeric systems are increasingly finding favor due to their potential for rapid prototyping and high volume manufacturing using techniques that minimize reliance on the costly semiconductor process infrastructure. Nevertheless, each of these materials systems suffers from intrinsic limitations that constrain the applications space in which they can operate. This therefore provides the impetus for further development of alternative materials systems for microfluidic applications.

One such alternative material system that shows promise is titanium. Unlike silicon and glass, titanium possesses high fracture toughness, which increases shock resistance and decreases sensitivity to stress concentration. This reduces the demand upon packaging for mechanical isolation, thus making titanium particularly attractive for portable device applications where mechanical robustness is required. Titanium also exhibits superior thermal stability

and solvent resistance relative to most common micromechanical polymers, such as PDMS, PMMA, and polycarbonate. These qualities therefore illustrate the potential of titanium for use in fabrication of microfluidics devices intended for long-term use in aggressive harsh environment applications, such as chemical processing or *in vivo* biomedical devices.

Recent advances in micromachining technology now make realization of this potential possible by enabling fabrication of high aspect ratio structures with micrometer to nanometer-scale feature sizes and vertical sidewalls in bulk titanium substrates (Aimi et al. 2004; Parker et al. 2005). In addition, the high toughness of titanium permits handling of thin foil substrates without the need for fixture or support, thus simplifying fabrication of complex 3D structures through multilayer lamination of free-standing foil substrates. Finally, utilization of conventional metallic fabrication processes, such as milling and stamping, provide the opportunity for tight integration of macro- and micro-scale structures, as well as high-rate material removal in areas where the precision of dry etching is not required. In this paper we present details of the application of these techniques towards fabrication of two types of titanium-based microfluidic devices used for experimental visualization of dielectrophoresis-based particle separation and manipulation.

2 Device design considerations

2.1 Dielectrophoretic force

Dielectrophoresis (DEP) is a phenomenon in which motion of polarizable particles in a suspending medium is induced by the application of a non-uniform electric field. In the presence of an electric field gradient, the dielectrophoretic force is given by (Pohl 1978):

$$F_{DEP} = 2\pi v \varepsilon_m \alpha_r \nabla \left(E_{RMS}^2\right)$$

where ν is the volume of the particle, ε_m the permittivity of the medium, E_{RMS} is the RMS value of the electric field, and α_r the real part of the Clausius–Mosotti factor. The real component of the Clausius–Mosotti factor is given by:

$$\alpha_r = Re\left(\frac{\varepsilon_p^* - \varepsilon_m^*}{\varepsilon_p^* + 2\varepsilon_m^*}\right)$$

where ε_p is the particle dielectric constant and the star (*) denotes the complex quantity $\varepsilon^* = \varepsilon - i\frac{\sigma}{\omega}$ with σ the conductivity and ω the angular frequency. When α_r is positive, F_{DEP} is also positive, thus the particles are attracted toward the region of higher electric field gradient, i.e. the particles undergo positive DEP (P-DEP). Conversely, when α_r is negative, F_{DEP} is negative, therefore causing repulsion from the higher electric field gradient region, i.e. the particles undergo negative DEP (N-DEP). The frequency at which α_r=0 is called the crossover frequency, at this frequency there is no DEP-based force imposed on the particles.

The nature of the DEP force depends on a number of factors, including the temporal and spatial configuration of the applied electric field, and the dielectric properties of both the particles and the suspending medium. Using DEP, size and shape-based particle separation has been demonstrated (Randall et al. 1992), as well as trapping (Huang and Pethig 1991) and repulsion (Masuda et al. 1988) of various types bioparticles and molecules (Morgan and Green 2003; Huges 2003). It is well known that strong electric field gradients can also induce advective flow based on electrohydrodyamic effects (Morgan and Green 2003). Recently, it was demonstrated that the dynamical interaction between this flow and DEP force can be exploited to create new particle trapping mechanisms with considerable potential for application in micro- and nano-scale particle separation, concentration, and mixing (Tuval et al. 2005). Experimental validation of this trapping phenomenon was performed using the first of the titanium-based dielectrophoresis devices presented here.

2.2 Device design

In order to obtain sufficiently large electric field gradients with reasonable applied voltage, the first of the titanium-based DEP devices developed in this study relies on a commonly used interdigitated electrode array configuration (Pethig et al. 1992; Crew et al. 2007). The array is composed of 20-μm wide thin-film titanium electrodes with 40-μm pitch defined on a dielectric film that electrically isolates the electrodes from the underlying titanium substrate. As shown in Fig. 1(a), this electrode array is located on the floor of a 45 μm deep flow channel of 1 mm width and 6 mm length, referred to as a floor electrode device (FED).

Although DEP-based particle manipulation can be qualitatively demonstrated using the FED, quantitative measurement of the particle velocity field in the fluid column above the electrodes is not possible because the orientation of the electrode plane is normal to the viewing axis (*Z*-axis). Measurement of this particle velocity field requires direct visualization of the cross section of the fluid column above the electrode plane. Consequently, a second device geometry has also been developed in which the electrodes are defined in the vertical channel wall. As shown in Fig. 1(b), this configuration places the electrode plane parallel to the viewing axis, thus allowing direct visualization of particle motion above the electrode plane. In these devices, the electrodes are defined in the device

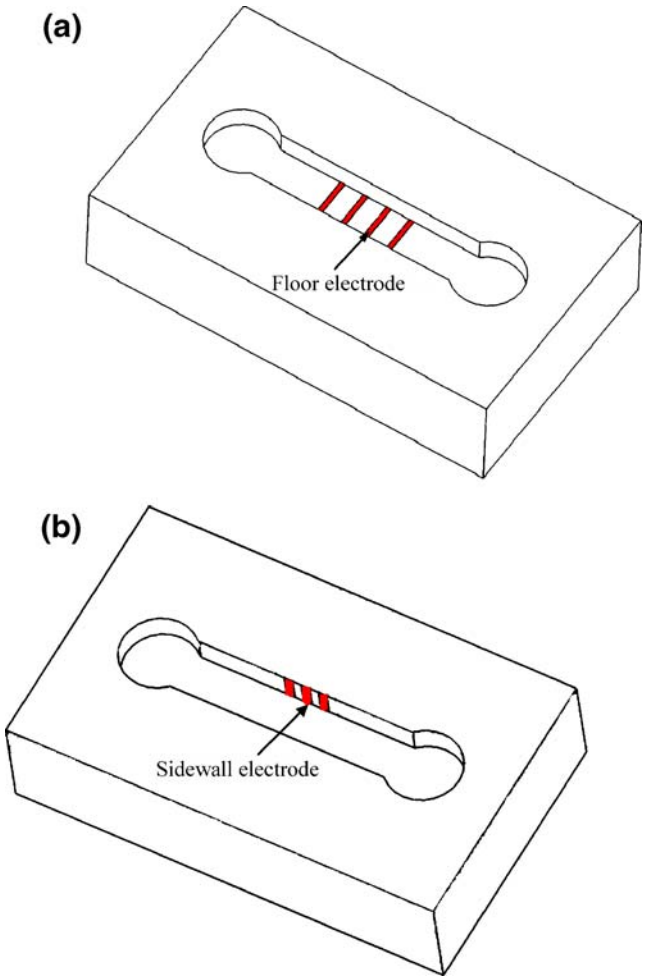

Fig. 1 Titanium DEP device schematics showing electrode configuration. (**a**) The floor electrode device, where electrodes are located on the floor of the flow channel; and (**b**) the sidewall electrode device, where electrodes are embedded within one channel wall

layer of a titanium-on-insulator substrate using trench isolation of 20-μm wide segments of the channel wall, referred to as a sidewall electrode device (SED). The flow channel dimensions used in the SED are 25-μm deep, 1-mm wide, and 6-mm long.

3 Fabrication

3.1 Floor electrode device

The fabrication process for the floor electrode device is outlined in Fig. 2. The process begins with deposition of a 1-μm thick layer of PECVD SiO_2 on a polished titanium substrate (Versalock VLR, Unaxis; deposition conditions: 100°C, 10 mT, SiH_4/Ar 250/20 sccm, 800 W ICP power, and 16 W RIE power). The substrate is 500-μm thick, grade 1 titanium (Tokyo Stainless Grinding Co., Ltd. Japan) with 10 nm RMS surface roughness, as measured by optical profilometry (Wyko NT1100, Veeco Metrology, Pennsylvania, USA).

Surface preparation prior to deposition of the electrical isolation layer is critical for DEP-based devices. It is found that often there is a short circuit between the electrode and the underlying titanium substrate when the titanium surface is only cleaned by solvents and plasma O_2 treatment. The problem was solved by adding an *in situ* argon plasma-cleaning step before silicon dioxide film deposition. The plasma treatment removes ionic contamination as well as native oxide, thus improving the adhesion of silicon dioxide thin film to the underlying bulk titanium substrate (Aronsson et al. 1998). A 300 s plasma treatment (10 mT chamber pressure, 30 sccm Ar, 800 W ICP power, and 20 W RIE power) is generally sufficient for such purposes.

The floor-based electrodes were formed by a lift-off process using negative tone photoresist (AZ 5214 photoresist, MicroChemicals), as shown in Fig. 2(b). A 3 min, 120°C post-development bake was required to prevent stripping of the photoresist during the subsequent metallization. Metal deposition was carried out by electron-beam evaporation of a 400-nm titanium thin film (CHA SEC600 Multi-Wafer Evaporator). After electrode deposition, lift-off was performed by soaking the sample in acetone with ultrasonic agitation for 20 min. Between the two electrode layers, a 300-nm thick silicon dioxide isolation layer was deposited using the same deposition recipe as described above and is lifted-off by soaking in photoresist stripper (PRX-127, Shipley) for 30 min at 80°C, followed by ultrasonic agitation for 10 min.

As seen in Fig. 2(c–e), the reservoirs and channel were fabricated separately in a 25-μm thick titanium foil (99.6% commercially pure Ti, annealed, Goodfellow Corp). A 1.3-μm thick TiO_x etch mask was first deposited on the thin foil substrate by DC reactive sputtering (Endeavor 3000 Cluster Sputter Tool, Sputtered Films, Inc.). The reservoirs and channel were then patterned using a positive photoresist (SPR 220–3.0, Shipley) and dry etched for 10 min using CHF_3-based chemistry (E640 ICP Etcher, Panasonic Factory Solutions; etch conditions: 1 Pa chamber pressure, 40 sccm CHF_3, 500 W ICP power, and 400 W RIE power) to transfer the channel pattern to the titanium oxide layer, as seen in Fig. 2(d). The pattern was then transferred completely through the titanium foil [Fig. 2(e)] using the TIDE process, which is a highly anisotropic Cl/Ar-based dry etch (E640 ICP Etcher, Panasonic Factory Solutions; etch conditions: 2 Pa chamber pressure, 100/5 sccm Cl_2/Ar, 500 W ICP power, and 100 W RIE power). This process yielded vertical, scallop-free sidewalls at etch rates in excess of 2 μm/min, depicted in Fig. 3.

Once the reservoirs and channel were defined, the through-etched thin foil substrate was bonded to the electrode substrate via photosensitive BCB-based adhesive

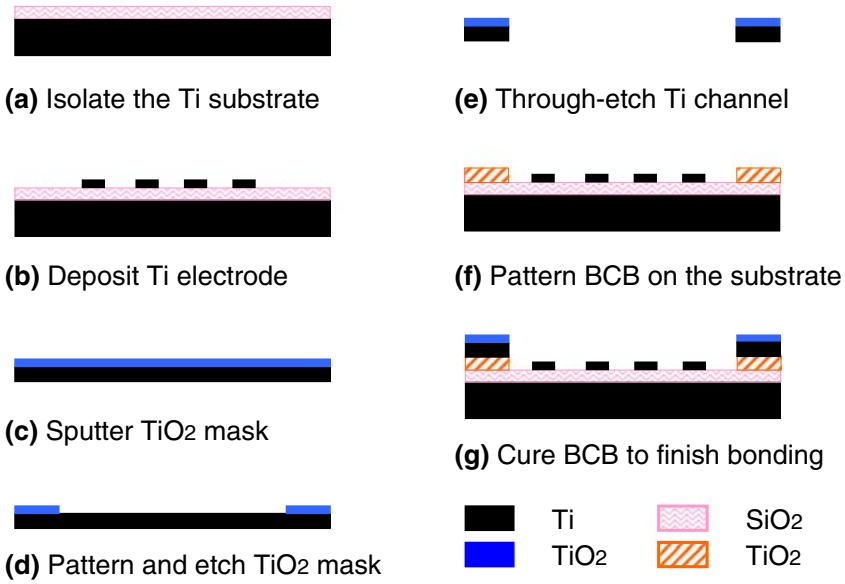

Fig. 2 Process flow of the titanium floor electrode device. Thin film titanium electrodes are patterned on an insulated titanium substrate and then bonded to a through-etched titanium microchannel using polymer (BCB) adhesive bonding. (**a**) Deposit a 1-μm thick layer of PECVD SiO_2 on a polished titanium substrate; (**b**) floor-based electrodes were formed by a lift-off process using negative tone photoresist; (**c**–**e**) the reservoirs and channel were fabricated separately in a 25-μm thick titanium foil; (**f**/–/**g**) through-etched thin foil substrate was bonded to the electrode substrate via BCB-based adhesive

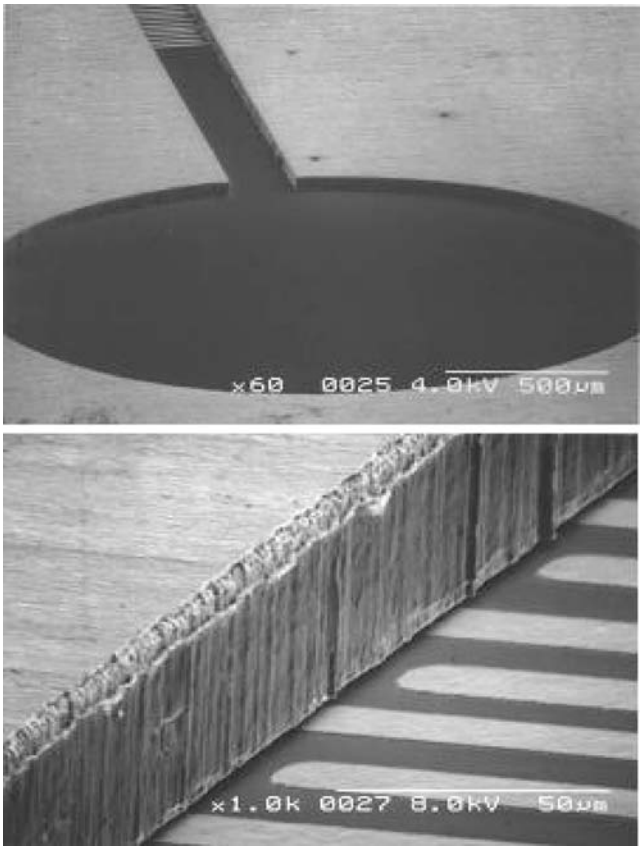

Fig. 3 Low and high magnification scanning electron micrographs of the reservoir and channel of the Floor Electrode Device with 24 electrodes located at the bottom of the channel (before macro-machining of the reservoir to form vertical fluidic interconnect to the fluid supply stage)

(Cyclotene 4026, Dow Chemical), as seen in Fig. 2(f) and (g). The BCB adhesive is electronically insulating and photo-definable, thus simplifying fabrication and enabling electrical isolation without the need for further SiO_2 deposition steps. It also requires relatively low bond force and low bonding temperature, thus helping preserve the integrity of the underlying metal and dielectric layers. After applying an adhesion promoter (AP 3000, Dow Chemical) on the electrode substrate, BCB was spin-coated at 4,000 rpm for 30 s; then the specimen was soft-baked in a 70°C convection oven for 20 min. Afterwards, the BCB was exposed using a contact aligner for 100 s at a UV intensity of 7.5 mJ/cm^2. Puddle development was then performed using DS 2100 developer for 150 s and the chip is spun dry at 2,000 rpm for 30 s. The same procedure was repeated on the through-etched foil substrate as well. To complete the bonding, the two substrates were aligned and tacked using a contact aligner and then cured in a nitrogen purged convection oven at 150°C for 2 h. The final BCB bond layer thickness was ~20 μm. Although the recommended full curing temperature for BCB is 250°C, use of such high temperatures resulted in electrical shorting due to cracking of the insulating silicon dioxide layers caused by the large thermal mismatch between BCB (42 ppm/°C) and silicon dioxide (0.5 ppm/°C). Reduction of the bonding temperature to 150°C mitigated mismatch-induced stress while still providing for sufficient bond strength to ensure leak-free performance.

After adhesive bonding, the device was coated with a 7-μm thick photoresist layer (SPR 220–7.0, Shipley), and

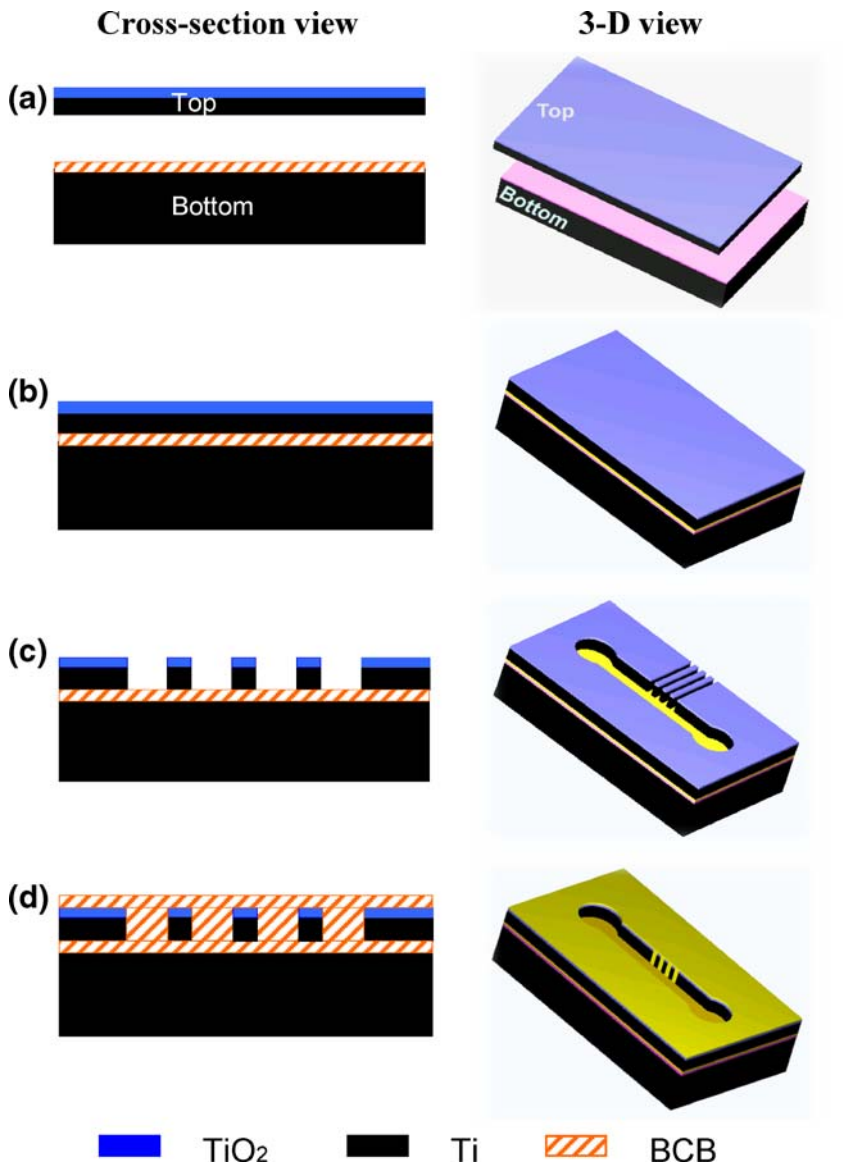

Fig. 4 Bulk titanium sidewall electrode device process flow. (**a**) Insulation of titanium substrate and sputtering of the mask material on titanium foil; (**b**) BCB bonding to form the titanium on insulator substrate; (**c**) transfer of channel, electrode, and contact pad patterns to the titanium oxide mask with a CHF_3-based dry etch, followed by deep etching of the titanium foil with Cl-based dry etch; and (**d**) coating with BCB to fill the trenches, followed by lithographic patterning to remove BCB in the channel and reservoirs

the fluid inlet and outlet reservoir features were lithographically patterned. Afterwards, the two reservoirs were macromachined through the thickness of the titanium electrode substrate using a conventional drill press, with the photoresist serving as a protective layer. The ability to combine both micromachining and conventional macromachining demonstrates one of the advantages of bulk titanium as a microfluidic material, particularly with regard to the time and cost saving associated with high-rate raw material removal.

3.2 Sidewall electrode device

Fabrication of the sidewall electrode device relied on creation of a-titanium-on-insulator (TOI) substrate, as shown in Fig. 4. First, a 1-μm thick PECVD silicon dioxide layer was deposited on the thick titanium substrate. Similarly, a 1.3-μm thick titanium oxide film was sputtered on a separate 25-μm thick titanium foil as shown in Fig. 4(a). Next, BCB adhesive was spun onto the thick titanium substrate and the coated substrate was bonded to the titanium foil [Fig. 4(b)]. Patterns for the microchannel, fluid reservoirs, electrodes, and contact pads were defined on the device layer of the TOI substrate using positive tone photoresist (SPR 220–3.0). These patterns were transferred to the titanium oxide mask using CHF_3-based dry etching, and then transferred into the titanium foil using the TIDE process. The titanium device layer was etched until the underlying bonding material (BCB) is exposed [Fig. 4(c)]. Thin film deposition, adhesive bonding, and the TiO_x/Ti etching recipes were the same as those used in the fabrication of the floor electrode device. Following etching, photosensitive BCB was used to planarize the etched structures and was then removed from the flow channel

and reservoirs by a second lithographic exposure and development process, as shown in Fig. 4(d). After applying adhesion promoter (AP3000), BCB (Cyclotene 4026) was spin-coated at 1,500 rpm for 30 s, followed by 90 s hotplate soft-bake at 90°C. Exposure was performed using a contact aligner (MJB 3 UV400 IR, Suss Microtec, Germany) with a dose of 7.5 mJ/cm^2/s for 150 s. The exposed resist was developed by immersion in heated DS 3100 solution for 4 min, followed by washing in unheated DS 3100 solution for 2 min, and spin drying at 1,000 rpm for 30 s. The sample was then cured in an inert gas oven 150°C for 2 h. Afterwards, the sample was protected with photoresist and the fluidic interconnects are drilled using the same procedure described for the floor electrode device.

4 Experiment results

4.1 Experimental apparatus

A Plexiglas fluid supply stage, shown in Fig. 5, was used to guide the fluid into both types of titanium DEP devices via the drilled fluidic interconnects. A 1-mm thick PDMS layer was used to cover the channel and reservoirs to prevent evaporation while allowing for optical detection. This sealing is not permanent which therefore allows for convenient cleaning of the device for subsequent experiments. Electrical connections were made using two card edge connectors (Digi-Key, Minnesota, USA) to connect the titanium chip to the electronic test equipment.

Imaging of particle motion was performed using an epi-fluorescence microscope (model ECLIPSE E600FN, Nikon) with a mercury arc lamp (HBO 100 w/2, OSRAM); the illumination intensity was controlled by a power stabilizer (1962LTS, Opti-Quip). Visualizations were made using a Nikon 20× water immersion lens with a working distance of 2 mm. A digital CCD camera (C7300, Hamamatsu) under software control (Digital Camera Control 4.0b17, Hamamatsu Photonic Corporation) was used to record particle images.

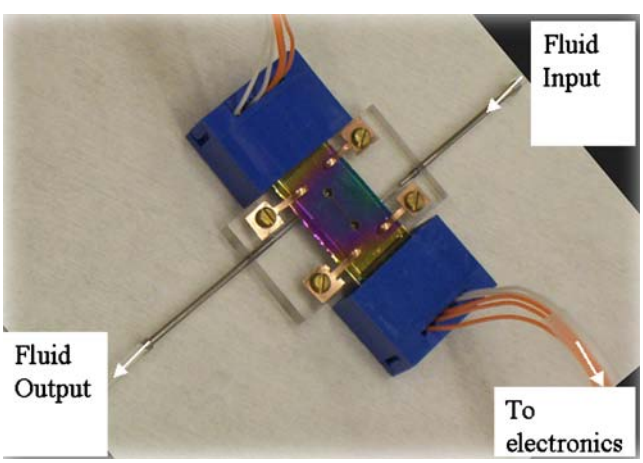

Fig. 5 Photograph of the assembled device for testing. The titanium DEP device is sealed by a 1-mm thick PDMS layer and sits on a fluid supply stage. Electrical connectivity is realized through two card edge connectors

Monodisperse green polystyrene fluorescence microspheres (Duke Scientific, California, USA, 0.1- to 5-μm diameter, 1.05 kg/m^3 density) were used in all particle manipulation experiments. These microspheres contain dye incorporated in the polymer matrix to produce a bright green color when excited by blue light. Before use, the beads were diluted to a low concentration (10^6 beads/ml) in de-ionized water. The conductivity of the solution was measured using a Hanna Primo 5 conductivity meter (Automated Aquarium Systems, California, USA).

During a typical experiment, the particle suspension was injected into the DEP device using a PHD 2000 syringe pump (Harvard Apparatus, Massachusetts, USA) at a flow rate of 30 μl/min. The flow was stopped once the suspension filled the channel. The suspension was then allowed to reach quiescence in the device for 10 min before the electric field was applied. A sinusoidal signal was applied with an 11 MHz function generator (Wavetek, model 21). The signal was monitored by an oscilloscope (Tektronix TDS 3012).

4.2 Two-frequency particle separation using the floor electrode device

The use of dielectrophoresis for microfluidic particle separations were studied extensively (Huges 2003). In most cases, for separations involving suspensions composed of mixtures of two types of particles (A and B), a single frequency, ω, was selected such that the two types of particles are subjected to differing DEP forces, e.g. "A" particles undergo P-DEP, while "B" particles undergo N-DEP. However, when the crossover frequencies of the two particles types were close, single frequency separations are often unable to provide sufficient distinction between the different particle types (Gascoyne et al. 2002). Theoretical studies (Chang et al. 2003) suggested that superposition of multiple frequencies may enable separation in instances such as these. Recent experimental work demonstrated that coupled negative DEP force from opposite sidewall electrodes can be used to separate cells continuously (Wang et al. 2007a). Using the titanium-based FED, we provided here two-frequency particle separation with floor electrode array.

To demonstrate the effectiveness of multi-frequency DEP separation we compared the behavior of a particle suspension composed of a bimodal particle mixture under the influence of both single frequency and multi-frequency excitation. The experimental conditions used in both sets of

experiments were as follows: 1.90 and 0.71-μm diameter monodisperse green fluorescence polystyrene spheres; 12 μS/cm suspension conductivity; and 10 V pk–pk excitation voltage. As seen in Fig. 6(a), in the absence of applied voltage, both large and small particles were observed to be randomly distributed in the focal plane (microscope was focused on the floor of the flow channel where the electrodes are located). Upon application of dual-frequency excitation at 100 kHz and 1 MHz to the electrode simultaneously [Fig. 6(b)], repulsion of the large particles away from the electrodes was observed (N-DEP), as evidenced by their movement out of the focal plane. Although not as obvious, attraction of the smaller particle towards the edges of the electrodes (P-DEP) was also observed. Separation of the differing diameter particles was therefore clearly apparent. In contrast, similar experiments (data not shown) performed with single frequency excitation at either 100 kHz or 1 MHz showed that both types of particles underwent similar forces and, thus, were not separated. This demonstrated the efficacy of dual frequency DEP for difficult separations.

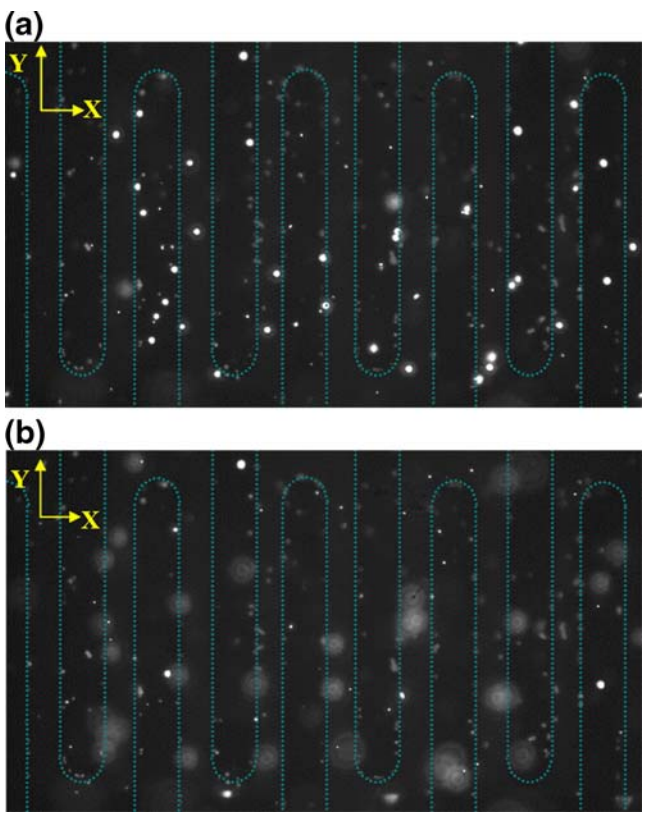

Fig. 6 Optical fluorescence images of particles in the channel of the floor electrode device. Images taken with CCD positioned normal to device plane, looking down on the channel, with focal plane at the electrodes on the bottom of the channel. The location of the electrodes is designated by *dotted lines*. The electrodes are 20-μm wide with 40-μm pitch. The electric field is off in (**a**). Superimposed 10 V peak-to-peak waveforms of 100 kHz and 1 MHz are applied in (**b**) causing repulsion of larger particles away from focal plane

It is important to note that the observed motion of the particles under dual-frequency excitation was not resultant from Brownian motion, nor was it induced by global flow in the chamber. As mentioned earlier, sufficient time was given after introduction of the suspension into the flow channel to allow quiescent conditions to be established before application of excitation voltage. Further, Brownian motion of the particles during this quiescent period did not produce particle motions with displacements of the magnitude seen during excitation. Finally, it should be noted that a small number of particles are observed to be immobile under the applied excitation in Fig. 6. This was presumably due to their adhesion to the substrate prior to the application of excitation voltage.

4.3 Z-dimension flow visualization using the sidewall electrode device

It is apparent from Fig. 6 that the FED only allows qualitative assessment of the influence of DEP forces on particles. Although the movement of particles within the focal plane can be accurately tracked, tracking of particle motion on other planes is not possible. Visualization of particle motion in the plane normal to the electrode plane (and normal to the long axis of the electrode line as well) is particularly important in this regard, as this is the plane that enables best assessment of the affect of the electric field on particle motion. The electrode configuration provided by the SED aligns the electrode plane with the microscope viewing axis. This therefore enables high-resolution, quantitative visualization of particle motion in the fluid column above the electrode plane using micro Particle Image Velocimetry (μ-PIV), as will be demonstrated below.

The principle of μ-PIV is based on spatial correlation of particle displacements measured within cells taken from successive video image frames. The vector velocity associated with the cells is calculated based on the time interval between two images. The μ-PIV method thus gives the 2D velocity field in the considered plane. For higher resolution, several time-sequences of images are correlated and ensemble-averaged to obtain the 2D velocity fields (Meinhart et al. 2000). Further discussion of the μ-PIV method can be found in the literature (Santiago et al. 1998 and Meinhart et al. 1999).

The experimental apparatus and conditions used for particle flow visualization and μ-PIV measurements with the SED were similar to those used for the floor electrode device. The SED was attached to the fluidic supply stage and an aqueous suspension (32 μS/cm) composed of 0.7 μm diameter monodisperse green fluorescent polystyrene particles was introduced into the flow channel. Once quiescence was achieved the SED electrodes were energized such that the middle electrode was held at a higher

electrical potential than the neighboring electrodes. Imaging was performed using the same fluorescence microscope described earlier, with dual-head Nd:YAG laser excitation (New Wave Research, Model MiniLase II 30) and a different CCD camera (PIVCAM 13-8, model 630047, TSI, Minnesota, USA).

Experimental observations indicated that particle motion began to occur when the applied potential exceeded 7 V pk–pk. Under applied excitation frequencies ranging from 1 to 2 MHz, positive dielectrophoresis was observed to dominate, thus causing particles to accumulate at the electrodes (data not shown). For frequencies in excess of 2 MHz, however, negative-DEP phenomena were observed, as shown in Fig. 7(b). In this figure, taken 6 s after application of 20 V pk–pk excitation at 10 Mhz, a semi-ellipse frontier was observed to form and steadily move away from the electrodes. This frontier corresponded to the depletion of particles in the suspension in the vicinity of the electrodes, due to N-DEP-induced repulsion. Figure 7(c) showed raw μ-PIV data resulting from averaging over 100 continuous images taken at a rate of 33 frames per second, without smoothing or removing erroneous velocity vectors.

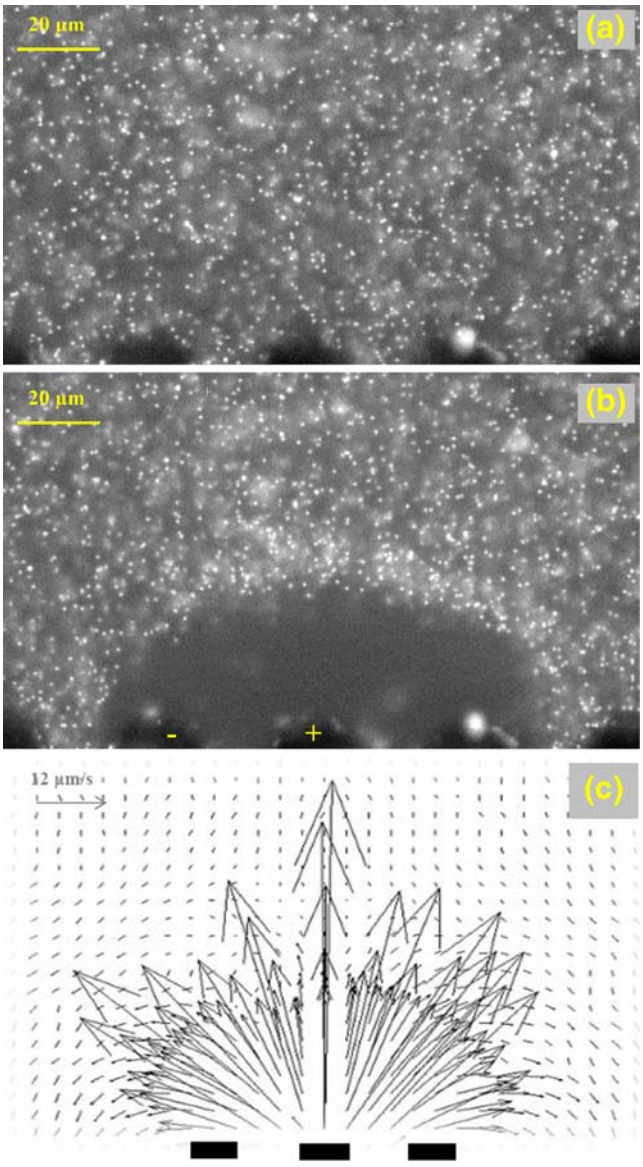

Fig. 7 Visualization of negative dielectrophoresis-induced particle motion in the sidewall electrode device. (**a**) Fluorescence image of initial status when the electric field is not applied; (**b**) Fluorescence imaging of 0.7-μm diameter polystyrene particles motion under 20 V pk–pk excitation at 10 MHz; (**c**) Particle velocity filed obtained using μ-PIV measurement. The *black bars* represent the electrodes which are 20 μm in width

5 Discussion

As demonstrated here, titanium offers a number of unique and potentially enabling advantages relative to prevailing materials used for DEP-based devices. With regard to process simplification and design capability, chief among these is the ability to easily stack and bond pre-fabricated titanium foils and substrates. Due to the high fracture toughness of titanium, foils thicker than 25 μm can be processed without the need for carrier wafers. In the example of the floor electrode device, the ability to bond the pre-fabricated channel layer foil substrate to the patterned electrode substrate makes fabrication of complex 3D microfluidic structures with DEP function a relatively easy process. Similar multi-layer bonding operations are possible in conventional materials systems (e.g. Si and glass), however, the intrinsic brittleness of these materials complicates processing by requiring use of temporary fixation for support of thin delicate device layers. Furthermore, device yield is reduced considerably due to the increased potential for fracture during bonding.

In the case of the sidewall electrode device, the use of titanium as both structural and electrical element provides a number of benefits relative to other previously reported devices. All device elements are defined in the device layer of the TOI substrate, which therefore eliminates the complexity associated with lithographic patterning of electrodes on the channel walls (Pai et al. 2002; Honda et al. 2003; Wang et al. 2005). Furthermore, titanium's intrinsic toughness provides a more mechanically robust device structure than similar devices fabricated in silicon on insulator substrates (Zhang et al. 2004; Iliescu et al. 2005). Finally, the dual-mask process developed for the Ti-SED reduces process complexity considerably relative to other similar devices (Iliescu et al. 2005; Wang et al. 2007b).

In addition to the specific benefits associated with the devices demonstrated here, titanium offers further advantage with regard to the breadth of potential applications which its use might enable. For example, its high toughness imparts mechanical robustness that is otherwise lacking in

brittle materials such as silicon and glass. This therefore minimizes the need for packaging to mitigate mechanical stresses, thus reducing device cost and complexity, as well as potentially enabling more direct exposure to the surrounding environment for enhanced sensitivity in applications such as environmental monitoring. Moreover, the multi-layered fabrication capability provided by titanium's toughness may facilitate development of robust, complex, highly integrated, multifunctional microfluidic devices with far greater device densities than conventional 2-D integration schemes. The promise of such integration has been recently demonstrated in polymeric devices (Thorsen et al. 2002). However, reliance upon polymeric materials limits the application space within such devices, due to issues such as high gas permeability and limited solvent resistance. Titanium also provides far superior thermal conductivity to that of the glass and most commonly used polymers, thus making it a good candidate for systems that require rapid creation and dissipation of thermal energy, such as those used for energy conversion or chemical processing. Finally, titanium's superior biocompatibility makes it a highly attractive material for biomedical microfluidic applications as well. Recent demonstration of promise in this regard can be seen in the titanium-based microneedle devices developed by Parker et al. (2007).

6 Conclusion

The viability and feasibility of bulk titanium as an alternative material platform for microfluidic devices were demonstrated through the fabrication of two types of devices for dielectrophoresis-based particle manipulation. The high fracture toughness of titanium enables simplified multi-layer processing which therefore provides capability for design of complex device structures that would be otherwise difficult, if not impossible to achieve in prevailing micromechanical material systems. Using these devices, two-frequency dielectrophoretic separation of binary microparticle suspensions, as well as high resolution imaging of the particle motion above the electrode plane were demonstrated. These demonstrations illustrate the potential provided by titanium for the simplified fabrication of robust microfluidic devices with unique functionalities that cannot be achieved with other conventional materials systems.

Acknowledgment The authors acknowledge the National Science Foundation NIRT program for financial support of this work. The authors would also like to thank Prof. Carl Meinhart, Dr. Garrett D. Cole and Mr. Dave Bothman for their helpful discussions.

References

M.F. Aimi, M.P. Rao, N.C. Macdonald, A.S. Zuruzi, D.P. Bothman, Nat. Mater. **3**(2), 103 (2004)
B.O. Aronsson, J. Lausmaa, B. Kasemo, J. Biomed. Mater. Res. **35** (1), 49 (1998)
D.E. Chang, S. Loire, I. Mezic, *Proceedings of 42nd IEEE Conference on Decision and Control (CDC 2003), Maui, Hawaii*, **6**, 6448 (2003)
N. Crew, J. Darabi, P. Voglewede, F. Guo, A. Bayoumi, Sens. Actuators, B, Chem. **125**(2), 672 (2007)
D. Figeys, D. Pinto, Anal. Chem. **72A**, 330 (2000)
P.R.C. Gascoyne, J. Vykoukal, Electrophoresis **23**, 1973 (2002)
C. Ho, Y. Tai, Annu. Rev. Fluid Mech. **30**, 579 (1998)
N. Honda, K. Emi, T. Katagiril, T. Irital, S. Shojil, H. Sato, T. Homma, T. Osaka, M. Saito, J. Mimo, Y. Wada, *Proceedings of the 12th International Conference on Solid Slate Sensors, Actuators and Microsystems*, Boston. June 8–12, 1132 (2003)
Y. Huang, R. Pethig, Meas. Sci. Technol. **2**, 1142 (1991)
M.P. Huges, *Nanoelectromechanics in Engineering and Biology* (CRC Press LLC, Boca Raton, FL, 2003)
C. Iliescu, G.-L. Xu, V. Samper, F.E.H. Tay, J. Micromechanics Microengineering **15**(3), 494 (2005)
S. Masuda, M. Washizu, I. Kawabata, IEEE Trans. Ind. Appl. **24**(2), 217 (1988)
C.D. Meinhart, S.T. Wereley, J.G. Santiago, Exp. Fluids **27**, 414 (1999)
C.D. Meinhart, S. Wereley, J. Santiago, J. Fluids Eng. **122**(2), 285 (2000)
H. Morgan, N.G. Green, *AC Electrokinetics: Colloids and Nanoparticles* (Research Studies Press LTD, Taunton, 2003)
R.S. Pai, T.J. Roussel, M.M. Crain, D.J. Jackson, R.P. Baldwin, R.S. Keynton, J.F. Naber, K.M. Walsh, *Proceedings of the second joint EMBS/BMES Conference*, Houston TX, USA, October 23–26 (2002)
E.R. Parker, M.F. Aimi, J. Thibeault, M.P. Rao, N.C. MacDonald, J. Electrochem. Soc. **152**(10), C675 (2005)
E.R. Parker, M.P. Rao, K.L. Turner, C.D. Meihart, N.C. MacDonald, J. Microelectromech Syst. **16**(2), 289 (2007)
P. Pethig, X Wang, Y. Huang, J.P.H. Burt, J. Phys. D: Appl. Phys. **25**, 881 (1992)
H. A. Pohl, *Dielectrphoresis* (Cambridge University Press, Cambridge, 1978)
C.A. Randall, S. Miyazaki, K.L. More, A.S. Bhalla, R.E. Newnham, Mater. Lett. **15**(1–2), 26 (1992)
J.G. Santiago, S. Wereley, C.D. Meinhart, D.J. Beebe, R.J. Adrian, Exp. Fluids **25**, 316 (1998)
H.A. Stone, A.D. Stroock, A. Ajdari, Annu. Rev. Fluid Mech. **36**, 381 (2004)
T. Thorsen, S.J. Maerkl, S.R. Quake, Science **298**, 580 (2002)
I. Tuval, I. Mezic, F. Bottausci, Y.T. Zhang, N.C. MacDonald, O. Piro, Phys. Rev. Lett. **95**(23), 2360021 (2005)
W. Z. Wang, M. Sigurdson, C.D. Meinhart, Exp. Fluids **38**, 1 (2005)
L. Wang, L. Flanagan, A.P. Lee, J. Microelectromech Syst. **16**(2), 454 (2007a)
L. Wang, L.A. Flanagan, N.L. Jeon, A.P. Lee, Lab. Chip **7**(11), 1114 (2007b)
Y.T. Zhang, H. Chen, I. Mezic, C.D. Meihart, L. Petzold, N.C. MacDonald, *Technical Proceedings of the 2004 NSTI Nanotechnology Conference and Trade Show*, Boston, March 7–11th **I**, 292 (2004)